Nanoscale

Structure-property correlations in a phase-pure high-temperature superconductor with a record BCS Tc = 55 K

Journal:	*Nanoscale*
Manuscript ID	NR-ART-01-2019-000562.R1
Article Type:	Paper
Date Submitted by the Author:	28-Mar-2019
Complete List of Authors:	Bhaumik, Anagh; North Carolina State University, Department of Materials Science and Engineering Narayan, Jagdish; North Carolina State University , Materials Science and Engineering

Structure-property correlations of a phase-pure high-temperature (T_c = 55 K) superconductor: B-Doped Q-Carbon

Anagh Bhaumik[1], Jagdish Narayan[1*]

[1]Department of Materials Science and Engineering, Centennial Campus

North Carolina State University, Raleigh, NC 27695-7907, USA

*Correspondence to: narayan@ncsu.edu

Abstract

Here, we report the detailed structure-property correlations of a phase-pure B-doped Q-carbon high-temperature superconductor having a superconducting transition temperature (T_c) of 55 K. This superconducting phase is a result of nanosecond laser melting and subsequent quenching of a highly super undercooled state of molten B-doped C. The temperature-dependent resistivity at different magnetic fields and magnetic susceptibility measurements indicate a type-II Bardeen-Cooper-Schiffer superconductivity in B-doped Q-carbon thin films. The magnetic measurements indicate that the upper and lower critical fields follow $H_{c2}(0)[1-(T/T_c)^{1.77}]$ and $H_{c1}(0)$ $[1-(T/T_c)^{1.19}]$ temperature dependence, respectively. The structure-property characterizations of B-doped Q-carbon indicate a high density of electronic states near the Fermi-level and large electron-phonon coupling. These factors are responsible for *s*-wave bulk type superconductivity with enhanced T_c in B-doped Q-carbon. The time-dependent magnetic moment measurements indicate that B-doped Q-carbon thin films follow the Anderson-Kim logarithmic decay model having high values of pinning potential at low temperatures. The crossover from two-dimensional to three-dimensional nature of Cooper pair transport at T/T_c = 1.02 also indicates a

high value of electron-phonon coupling which is also calculated using the McMillan formula. The superconducting region in B-doped Q-carbon is enclosed by T_c = 55.0 K, $J_c = 5.0 \times 10^8$ A/cm^2, and H_{c2} = 9.75 T superconducting parameters. The high values of critical current density and pinning potential also indicate that B-doped Q-carbon can be used for persistent mode of operation in MRI and NMR applications. The Cooper pairs which are responsible for the high-temperature superconductivity are formed when B exists in the sp^3 sites of C. The electron energy loss spectroscopy and Raman spectroscopy indicate a 75% sp^3 bonded C and 70% sp^3 bonded B in the superconducting phase of B-doped Q-carbon which has 27 at% B and rest C. The dimensional fluctuation and magnetic relaxation measurements in B-doped Q-carbon indicate its practical applications in frictionless motors and high-speed electronics. This discovery of high-temperature superconductivity in strongly-bonded and light-weight materials by using non-equilibrium synthesis will provide the pathway to achieve room-temperature superconductivity.

Introduction:

The hybridization of *s* and *p* orbitals in C atoms can lead to the formation of various allotropes and phases which have interesting magnetic and electrical properties. The evolution of high-temperature superconductivity in C is due to its light-weight strongly-covalent bonded atoms and large Debye temperature (θ_D). The superconducting transition temperature (T_c) can be further increased by doping C structures thereby forming high density of electronic states ($N(0)$) near the Fermi energy level (E_F) with moderate to large electron-phonon coupling.[1] The van Hove singularities in low-dimensional C structures can also introduce high electronic density of states near E_F.[2] The superconductivity in carbon-based materials has been experimentally reported in graphite intercalation compounds at high pressure (CaC_6, T_c = 15 K at 7.5 GPa),[3] single-walled carbon nanotubes (T_c = 20 K),[4] multi-walled carbon nanotubes (T_c = 12 K),[5] alkali metal-doped C_{60} (T_c = 33 K),[6] K-intercalated picene (T_c = 18 K),[7] B-doped diamond (T_c = 11 K)[8], *etc*. The superconductivity in the carbon-based materials follows the well-established Bardeen–Cooper–Schrieffer formalism where T_c is governed by the equation: $T_c = 1.13\theta_D e^{(-1/N(0)V)}$, where V denotes the Cooper pairing potential. Recently, a unconventional superconductivity (T_c = 1.7 K) is also demonstrated in the interface states of graphene layers twisted at an angle of 1.1^0.[9] The discovery of high-temperature superconductivity below 203 K in H_2S under high-pressure has stimulated significant research in light weight, strongly-bonded, and strongly-correlated electron-phonon systems.[10] Therefore, for carbon-based superconductivity, B-doped diamond was an optimal choice where increasing B concentration in the substitutional sites increased T_c from 4 to 11 K.[8,11] Though theoretical predictions claim that T_c in B-doped diamond can be increased up to 55 K with ~ 20 at% B,[1] but experimentally the increase in B beyond 5 at% presents formidable challenges in terms of internal strains, dopant clustering, and thermodynamic solubility limits.[12]

Therefore, highly non-equilibrium methods (based upon energetics of plasma and lasers) and strongly-bonded light weight amorphous materials are required to attain high-temperature superconductivity.

Recently, we have reported the formation of novel phase of carbon (Q-carbon) and BN (Q-BN) by melting and subsequent quenching of highly undercooled state of molten C and BN, respectively by using a high-powered nanosecond ArF excimer laser.[13,14] The Q-carbon phase is a new state of carbon with distinct structure and entropy, and contains four-fold sp^3 (75-85%) and rest three-fold sp^2 bonded carbon. The formation of the highly dense and amorphous Q-carbon phase is dependent on the degree of undercooling which is controlled by laser energy density and thermal conductivities of the substrate and the as-deposited thin film. Theoretical calculations and experimental evidence have also proved that the thermal conductivity of Si plays an important role in determining the degree of undercooling.[15] The process of undercooling is similar to applying high pressure and therefore it leads to the formation of strongly-bonded light weight materials having moderate to strong electron-phonon coupling. Undoped Q-carbon is a room-temperature ferromagnet,[16] which turns into a superconductor upon B-doping. We have reported high-temperature superconductivity in B-doped Q-carbon having T_c of 36 K and 55 K.[17,18] But in our previous samples exhibiting T_c = 55 K, we had an additional layer of zone-refined B on the top and so the 55 K layer was part of a composite structure. Therefore, we were not able to carry out detailed transport measurements which are very critical for practical applications. Since the B-doped Q-carbon thin films (exhibiting T_c = 55 K) were not phase-pure, they did not exhibit optimum superconducting characteristics (sharp transitions, large critical current density, low flux creep, *etc*). In the present research, we have solved this problem and synthesized phase-pure 55 K B-doped Q-carbon superconducting thin films (with no B zone-

refined layer) which have shown superior superconducting properties. In this paper, we present details of experimental procedures, temperature- and field-dependent magnetization, critical current density *vs* temperature, resistance *vs* temperature at different magnetic fields, critical fluctuations, temperature-dependent flux creep, and structure-property correlations (Raman and electron energy loss spectroscopy, scanning electron microscopy, high-angle annular dark field microscopy, and electron diffraction) of phase-pure B-doped Q-carbon thin films. We have also discussed the origin and nature of BCS superconductivity in the B-doped Q-carbon thin films and their potential applications in superconducting devices. Therefore, we envisage that highly non-equilibrium processing techniques can lead to the development of potential high-temperature superconductors which can be directly used for practical applications.

Experimental procedure:

The pulsed laser deposition (PLD) is used to deposit alternating layers of boron and amorphous carbon thin films onto *c*-sapphire substrates. For the PLD process, KrF excimer laser (laser wavelength=248 nm, pulse duration=25 ns) is used. The total thickness of the films ranges from 400-500 nm. The B and C sector targets are mounted on the same target carrousel which is rotated using a stepper motor. The back surface of the B target should be properly flushed with the C target so that no ablation of C occurs when the laser beam is rastered on the B target. The substrate temperature and the operating pressure are maintained at 450 K and 1.0×10^{-7} Torr. This operating pressure is maintained by using an oil-free scroll pump and turbomolecular pump. Prior to the deposition, the B and C targets are pre-ablated by using the KrF nanosecond laser to remove loose particles and surface contaminants. Then the pulsed laser beam is rastered (repetition rate=10 Hz) through the C and B (sector) targets. The laser energy density used during the deposition process ranges from 3.0-3.5 Jcm^{-2}. Subsequently, these B-C thin films are

irradiated with nanosecond ArF excimer laser (laser wavelength=193 nm, pulse duration=20 ns). The laser energy density used ranges between 0.6-1.0 Jcm^{-2}. The pulsed laser annealing technique melts the B-C composite films in a highly undercooled state which is followed by quenching. The process is completed within 200-250 ns. This leads to the formation of superconducting B-doped Q-carbon thin films. By using the two-dimensional diffusion equation [$X=2(D*t)^{0.5}$], the diffusivity coefficient (D) is calculated as ~ 2×10^{-4} cm^2/sec which suggests melting and liquid phase diffusivity. This helps to incorporate B (in excess of its thermodynamic solubility limit) in the electrically active sites of sp^3-bonded C. The characterizations of the B-doped Q-carbon thins films were carried out by using Raman spectroscopy, FESEM, EELS, HAADF, SQUID magnetometer, and PPMS. The Raman spectroscopy was performed using a Alfa300 R superior confocal spectroscope which has a 200 nm lateral resolution. The Raman instrument was pre-calibrated by using crystalline Si sample that has a sharp Raman peak at 520.6 cm^{-1}. The FEI Verios 460 L was used to perform the high-resolution FESEM analysis, which has a sub-nanometer resolution. For preparing the cross-sectional TEM samples, FEI Quanta 3D FEG (having dual beam technology) was used. The focused ion beam damage was cleaned up by using a low energy (5 kV, 10 pA) ion beam. To acquire the HAADF and EELS we have used the aberration-corrected STEM-FEI Titan 80-300 electron microscope. Using the monochromator, the EELS was tuned up to provide an energy resolution of 0.15 eV. The electron probe current and collection angle used were 38 pA and 28 mrads, respectively. The JEOL 2000 FX electron microscope was used for performing the selected area electron diffraction (SAED) of the B-doped Q-carbon thin films. A 200 kV electron beam from a LaB6 source was used for the electron diffraction experiments. The magnetic measurements were performed in the SQUID Quantum design magnetic property measurement system (MPMS3).

Both the VSM and DC modes were used for the magnetic measurements. The samples were mounted parallel and 90 degrees to the applied magnetic field. The temperature stability in the magnetometer was ±0.5 % and the magnetic field uniformity is 0.01% over 4 cm (sample length). The magnetic field strength as high as 7 Tesla (with a field charging resolution of 0.33 Oe) was used to perform the field dependent measurements in B-doped Q-carbon samples. The magnetic flux creep measurements were carried out in a magnetic field of 1 T under isothermal conditions in SQUID magnetometer. The temperature-dependent resistance and critical fluctuation measurements were carried out in the physical property measurement system (PPMS) at different magnetic fields (1-7 T).

Results and discussion:

A. Magnetic measurements and correlations: The magnetization moment *vs* temperature plots in zero field cooled (ZFC) and field cooled (FC) conditions are shown in figure 1(a). The B-doped Q-carbon superconducting thin films are mounted parallel (0-degree) and perpendicular (90-degree) to the external magnetic field during the temperature-dependent magnetization measurements. The samples are cooled in an external magnetic field of 100 Oe during the FC measurements. It is clearly evident that there occurs a sharp decrease in the value of magnetic moment (to negative values) below 55.0 K which is the superconducting transition temperature of this material. This is also known as the Meissner effect where magnetic flux expulsion occurs when a sample is cooled below the superconducting transition temperature. Beyond the superconducting transition temperature there is no temperature dependence of magnetic moment which indicates a complete destruction of Josephson coupling (or superconductivity). A large difference in the magnetic moment values between the ZFC and FC curves indicates the presence of large flux pinning forces in the material (which cause the pinning of magnetic vortices). This

leads to trapping of magnetic flux in the FC condition thereby causing an upshift of the negative magnetic moments. The magnetic susceptibility (χ) of B-doped Q-carbon superconducting samples are calculated as ~ -0.05 and -0.09 emu $cc^{-1}Oe^{-1}$ for ZFC (0 degree) and ZFC (90 degree) at 5 K, respectively. The values of χ are calculated as ~ -0.03 and -0.04 emu $cc^{-1}Oe^{-1}$ for FC (0 degree) and FC (90 degree) at 5 K, respectively. The ZFC magnetization shows the flux exclusion from the B-doped Q-carbon sample, whereas the FC magnetization indicates the flux expulsion. Therefore, the shielding and superconducting volume fractions can be calculated from the ZFC and FC curves, respectively. The shielding fraction (-4π χ) is calculated to be 0.63 when the superconducting samples are mounted parallel to the magnetic field. A complete shielding occurs when the samples are mounted perpendicular to the field which is also the reason for the 94.5% increase in the negative magnetic moment at the perpendicular position (as compared to the parallel position). The superconducting volume (Meissner) percentages are calculated to be 37.68 % and 50.24 % for 0-degree and 90-degree orientations, respectively. The insets of figure 1(a) show temperature-dependent first-order and second-order derivatives of magnetic moment. The derivative method is usually used to calculate the line shapes, characteristic peaks, and crossover points which determine the characteristic superconducting parameters. The peak of the first-order derivative curve and the point at which the second derivative plot crosses the *x*-axis indicate the value of T_c (~55 K). The asymmetry of the transition is calculated to be 1.9×10^{-2} using the relation: (A-B)/(A+B). The ratio of the widths calculated from the derivative plots ($\Delta T / \Delta T'$) is 1.08 and it indicates the characteristics of the superconducting transition line shape. The line shape and asymmetry of the superconducting transition in B-doped Q-carbon samples indicate the presence of strong electron-phonon coupling which is also calculated using McMillan equation. Figure 1(b) indicates magnetic moment *vs* magnetic field at isothermal

conditions. As it is clearly evident from the figure that at room temperature, B-doped Q-carbon thin films exhibit a paramagnetic character. For temperatures below T_c, the superconducting thin films show a "butterfly-like" magnetic hysteresis character which is a characteristic of type-II superconductors. The M-H plots indicate an irreversible nature of the magnetic moment with increasing and decreasing magnetic field. This is attributed to intergranular and London currents (around the superconducting grains), which can trap the Abrikosov vortices and fluxons in an irreversible manner thereby causing a hysteresis behavior of the magnetic moment *vs* field plots.[19] Above T_c, there is a complete loss of the hysteresis behavior (paramagnetic nature) indicating a complete dissolution of the Josephson coupling in the superconducting grains of B-doped Q-carbon. The decrease in the absolute value of magnetic moment with increasing temperature in B-doped Q-carbon thin films is a characteristic property of superconducting materials.[20] The values of lower and upper critical fields (H_{c1}(T) and H_{c2}(T)) are calculated from the magnetic hysteresis loops. With increasing magnetic field, the value of magnetic moment increases up to a certain amount of field and then it decreases thereafter. The magnetic field value for the largest value of negative magnetic moment in the 4th quadrant denotes H_{c1}(T). The values of H_{c2}(T) are determined as the magnetic field at which the magnetic moment goes to zero. As it is evident from the isothermal M-H plots that the width of the plots decreases with increasing temperature. Figure 1(c) depicts the critical magnetic field *vs* temperature plots for the B-doped Q-carbon thin films. Three distinct regions namely superconducting, vortex, and normal states are found in the superconducting thin films thereby ascertaining a type-II BCS nature of superconductivity (in the thin films). The H_{c2}(T) is found to vary at a faster rate than predicted by the Werthamer-Helfand-Hohenberg (WHH) model. According to the WHH model, $H_{c2}(0) = -0.69(dH_{c2}/dT)T_c$, where dH_{c2}/dT denotes the slope at T_c. Therefore, the value of H_{c2}(0) is

calculated to be 11.23 T which is also shown in figure 1(c). In the case of B-doped Q-carbon thin films, the value of $H_{c2}(0)$ is calculated by using the power law: $\frac{H_c(T)}{H_c(0)} = 1 - (\frac{T}{T_c})^n$. The data points fit best to the value of n = 1.77 and the value of $H_{c2}(0)$ is calculated (as 9.75 T) from the intersection point of the upper critical curve with the Y axis. For the case of temperature-dependent H_{c1} plot, the data points fit best to the value of n = 1.19 and the value of $H_{c1}(0)$ is calculated as 1106.40 Oe. There is an upward curvature ~0 K in the case of $H_{c1}(T)$, which can be explained by the increased sp^2 contribution in the bonding of B-doped Q-carbon. The B in sp^2 electronic sites also increases the value of pinning potential which is explained in the flux creep section. The values of T_c calculated from the temperature-dependent upper and lower critical field plots are 55.45 and 54.99 K, respectively. The Ginzburg-Landau coherence length (ε_L) is calculated to be 58.10 Å by using the equation: $\varepsilon_L = [\Phi_0/2\pi H_{c2}(0)]^{0.5}$. In the above calculation, the values of $H_{c2}(0)$ and superconducting magnetic flux quantum (Φ_0) are taken to be 9.75 T and 2.07×10^{-15} T.m^2, respectively. The value of penetration depth (λ_d) is calculated to be 59.50 Å by using the equation: $H_{c1}(0) = (\Phi_0/4\pi\lambda_d^2)\ln(\lambda_d/\varepsilon_L)$. Therefore, the Ginzburg-Landau parameter (k) is calculated to be 1.02 ($>1/2^{0.5}$) thereby confirming that the B-doped Q-carbon thin films are type-II *s*-wave BCS superconductors. The Ginzburg-Landau parameter can also be calculated to be 1.04 by using the equation: $\frac{H_{c1}(0)}{H_{c2}(0)} = \frac{\ln(k)}{k^2 \times 2\sqrt{2}}$.[19] Therefore, similar values of k by using two different superconductivity equations instill the confidence about the superconconducting parameter calculations. The zero-temperature energy gap ($\Delta(0)$) in B-doped Q-carbon thin films is calculated as 8.50 meV by using the equation: $\Delta(0) = 1.8\ k_B T_c$. According to BCS formalism, the energy gap in superconductors is a region around the Fermi energy level containing high electronic density of states. The size of the energy gap (meV) is much smaller than the energy

scale of the band structure (eV). With increasing temperature, the superconducting energy gap decreases and vanishes above T_c giving rise to pseudogap states.

From the viewpoint of practical applications of a superconductor, it should have high values of upper critical field, transition temperature, and critical current density which is the maximum amount of dissipation less current that it can carry in the superconducting region. The critical current density (J_c) for the superconducting thin films is calculated using the Bean's formula: $J_c = \left[\frac{20\Delta M}{tw^2\left(l-\frac{w}{3}\right)}\right]$, where ΔM is the difference in magnetization values (+M and -M) at a particular magnetic field, and t, w, and l are the thickness, width, and length of the samples. The critical current density *vs* magnetic field plots at isothermal conditions are shown in figure 1(d). The value of J_c (0 Oe) at 5 K is calculated as 5.30×10^8 A/cm^2 which is considerably larger than in B-doped diamond[11] and other high-temperature superconductors.[21,22] Figure 1(d) shows a sharp decrease of J_c with increasing magnetic field at isothermal conditions. This is because at higher fields the Lorentz force, which is created on the magnetic vortices, causes depinning and thereby drastically reduces the critical current density. A smaller drop in J_c *vs* magnetic field plots (at a fixed temperature) is possible by introducing pinning centers which adversely affects T_c. A weaker dependence of J_c at higher fields is also observed in B-doped Q-carbon thin films. This can be due to the presence of a large number of weakly-coupled superconducting regions. The large values of J_c at lower temperatures are due to the presence of sp^2 bonded pinning states. The B-doped sp^2 entities present in the B-doped Q-carbon structure enhance the flux pinning. Therefore, high current density is required to move the pinned vortices. However at large magnetic fields this phenomenon is negligible due to the presence of an external magnetic field which assists the movement of the pinned states. It is well known that in the absence of flux pinning a superconductor exhibits low values of J_c due to the presence of flux lattice lines (FLL)

which dissipate the energy and the superconductor eventually turns "normal". The refinement of the superconducting grain size is, therefore, a viable approach to introduce pinning centers in a superconductor. This causes an increase in the value of J_c. But in the case of amorphous B-doped Q-carbon thin films, the non-magnetic inclusions (B-doped sp^2 entities) which are formed due to the ultrafast melting and quenching process, help to increase the value of J_c. The high values of J_c can also be predicted from the sharp fall in the magnetic moment below T_c and the large width of the magnetic moment *vs* field plots. The high critical current density of B-doped Q-carbon (at low magnetic fields) makes it an ideal candidate for low field NMR inserts. The temperature dependence of the critical field (at 0 Oe) is shown in the inset of figure 1(d). As it is evident from the figure that with increasing temperature, initially there is a sharp decrease in J_c which is followed by a gradual fall of J_c. This is due to the transition from Josephson coupling (at lower temperatures) to current-induced gap suppression effect (at higher temperatures). The value of J_c (0) is extracted as 7.10×10^8 A/cm^2 by extrapolating the curve to 0 K. At 5 K the value of J_c (0 Oe) is calculated as ~10^8 A/cm^2 which is one order magnitude higher than that found in YBCO, Nb-Ti, and Nb_3Sn high temperature superconductors.[23] The energy per unit volume (ΔG_{ns}) of the superconducting state relative to the normal state can be calculated by using the equation: $\Delta G_{ns} = -0.5\mu_0 H_c^2$,[22] where μ_0 and H_c denote magnetic permeability (in vacuum) and upper critical field (at ~0 K), respectively. The values of H_c in Nb_3Sn and B-doped Q-carbon are 27.0 T and 9.7 T, respectively. So, ΔG_{ns} (of B-doped Q-carbon) = 0.13 × ΔG_{ns} (of Nb_3Sn). Therefore, the high values of J_c in B-doped Q-carbon thin films are due to the fact that the energy required to exclude the magnetic field is extremely low in the case of B-doped Q-carbon (0.13 × energy required for Nb_3Sn superconductors). The depairing current density (j_0) in B-doped Q-carbon can be calculated by using $j_0 = \emptyset_0 / (3\sqrt{3}\pi\lambda^2\xi)$, where $\emptyset_0$, λ and ξ represent the flux quantum,

penetration depth and coherence length, respectively. The depairing current density is calculated as 1.55×10^{11} A/cm^2. Therefore, a further enhancement of the critical current density can be achieved in B-doped Q-carbon thin films by increasing the B concentration in the sp^2 electronic sites (which may further enhance number density of pinning centers). The high values of critical current density (~10^8 A/cm^2) and T_c (55 K) will enable B-doped Q-carbon power transmission (superconducting) cables to carry a large amount of dissipation-less current. The use of B-doped Q-carbon in power transmission and superconducting magnets will drastically decrease transmission losses (in the form of resistive heat) and cost of materials processing (carbon-based material). The large values of H_{c2} (9.75 T) in B-doped Q-carbon will also facilitate its use in superconducting supercolliders operating at liquid He temperature. B-doped Q-carbon will also find its application in He-based close-cycle refrigeration systems, operating above 10 K. This novel carbon-based material can also be used in MRI systems, where magnetic flux densities of ~2T are used. Since B-doped Q-carbon has extremely high values of T_c, J_c and H_{c2}, it can sustain high magnetic fields without losing its superconducting properties. These factors ultimately reduce the operational cost of superconducting-based frictionless motors.

The electron-phonon coupling parameter (for phonon-mediated BCS superconductivity) can be calculated using the McMillan formula $T_c = \frac{<\omega>_{\log}}{1.2}\exp\left(-\frac{1.04(1+\lambda)}{\lambda-\mu^*(1+0.62\lambda)}\right)$, where $<\omega>_{\log}$ is the logarithmic average of phonon frequencies, μ^* is the screened Coulomb pseudopotential, and λ is the measure of average electron-phonon coupling. Using the value of $<\omega>_{\log}$, μ^* and T_c as 67.4 meV, 0.1, and 55.0 K, respectively, the calculated value of electron-phonon coupling parameter (λ) is 1.01. The logarithmic average of phonon frequencies ($<\omega>_{\log}$) is calculated from temperature-dependent Raman spectroscopy of B-doped Q-carbon thin films. The Debye temperature (Θ_D) is related to $<\omega>_{\log}$ by the equation: $\Theta_D = 1.208 *$

$< \omega >_{log}$. The Raman shift (of the Raman-active vibrational mode centered ~1320 cm^{-1}) gradually turns from non-linear to linear region (at 315 K) with increase in temperature. This crossover temperature point is equal to ($\Theta_D/3$).[24] Therefore, the value of $< \omega >_{log}$ is calculated to be 67.4 meV. Presently, we are performing detailed specific heat measurements, temperature-dependent Raman measurements, and low-loss EELS measurements to determine the density of states near the Fermi energy level and compare with theoretical DFT calculations by Moussa and Cohen.[1] The details of the above-mentioned study will be reported elsewhere. This value of λ is also consistent with the theoretical calculations of Moussa and Cohen for highly B-doped diamond.[1] This value of λ is indicative of strong electron-phonon coupling in B-doped Q-carbon. The value of the electron-phonon coupling in B-doped amorphous Q-carbon is ~ 5 times than that in 2 at% B-doped diamond (T_c=4 K).[11] This suggests stronger electron-phonon coupling in B-doped Q-carbon as compared to B-doped crystalline diamond, thereby leading to high-temperature BCS superconductivity in B-doped Q-carbon. The BCS superconductivity can also be explained by the relation between λ, the density of states at the Fermi energy ($N(0)$), mass (M), average square of electron-phonon matrix element ($<I^2>$), and the characteristic phonon frequency averaged over the phonon spectrum ($<\omega^2>$). The average electron-phonon coupling parameter is related to the above three variables by the equation $\lambda = (N(0) < I^2 >)/(M < \omega^2 >)$. For the case of B-doped Q-carbon thin films, there is an increase in the value of N(0), the atomic mass is also quite low, and there exists strong covalent bonds. These factors cause an increase in the value of electron-phonon coupling parameter which along with the high dopant concentrations lead to high-temperature superconductivity in B-doped Q-carbon. Due to the presence of σ and π electronic states in B-doped Q-carbon, there can exist two distinct superconducting gaps. It has been shown that the critical magnetic fields can be analyzed

according to a theoretical model.[25] In this model, the σ and π electronic states are separated by a Josephson contact (interband coupling). At lower temperatures the contribution from the π electronic states are predominant, and this gives rise to an upward curvature in lower critical field in the doped thin films (having a significant π fraction). This can be explained by increased electronic scattering in the π band of the doped superconductor. As it is evident from the inset of figure 1(c), the H_{c1} follows an upward curvature at lower temperatures. This is due to the presence of π electronic states in B-doped Q-carbon, which also play an important role in critical current density and flux creep of this novel material.

B. Electrical measurements and correlations: Figure 2(a) depicts the sharp fall in resistance when B-doped Q-carbon thin films are cooled down below the superconducting transition temperature. The sharp transition is also indicative of homogeneous and bulk superconductivity in the thin films. The resistance *vs* temperature measurements are also performed at different magnetic fields. As it is evident from figure 2(a) that large magnetic fields are required to completely destroy the superconducting nature of B-doped Q-carbon. With increasing magnetic field, there occurs a lowering of T_c and broadening of transition width. This is a characteristic property of a high-temperature superconductor and it also helps us to calculate the value of upper critical field. To estimate the upper critical field (H_{c2}), we have used the power law $\frac{H_c(T)}{H_c(0)} = 1 - (\frac{T}{T_c})^2$. The extrapolated value of $H_{c2}(0)$ is calculated to be 10.0 T which is closer to the value of upper critical field calculated from the magnetic measurements. Figure 2(a) indicates a semiconducting nature of B-doped Q-carbon thin films above the superconducting transition temperature. Since, the thin films are heavily doped, they can be considered to be degenerate semiconductors. The superconducting degenerate semiconductors have strong intervalley and

intravalley electron-phonon coupling which assist in increasing the T_c. Theoretical calculations and experimental results have also suggested that high concentration of impurities in strongly bonded semiconductors leads to high temperature superconductivity.[26,27,28] The high dopant concentration in Q-carbon thin films gives rise to high density of electronic states near the Fermi level. This helps to increase the number of electronic states available for scattering which assists in increasing the BCS parameter (N(0)×V). The theoretical DFT calculations of Q-carbon and B-doped Q-carbon (T_c= 36 K) have already been reported.[29,30] In B-doped Q-carbon superconducting thin films, the high T_c is also caused by a large number of attractive intervalley phonons which increase the dielectric screening and reduce the repulsive Coloumb interaction. The electron-phonon coupling constant is large which also indicates a strong intervalley coupling in the novel superconducting material. Figure 2(b) shows a clear evidence of the onset of zero-resistance superconducting state below ~55 K. The onset of superconductivity ($T_{c\ on}$) and zero-resistivity ($T_{c\ off}$) conditions are observed at 59.8 and 55.4 K, respectively. The onset of superconductivity characterizes the critical fluctuations (formation and electrical transport of Cooper pairs) in a superconductor and are explained later. The sharp superconducting transition in B-doped Q-carbon indicates the presence of a high-quality superconducting phase. Figure 2(c) shows the first-order resistance-temperature derivative plot. The transition width (ΔT) is calculated to be 2.9 K. This transition width is comparable to that of high-temperature oxide superconductors[31] but much wider than that observed in single-crystal metallic superconductors (~10^{-4} K).[32] The transition width (at 0 T) is also dependent on the crystalline nature of a sample, with the single-crystal sample having a narrower transition than their polycrystalline or amorphous counterparts. Therefore, the transition width in B-doped Q-carbon is influenced by its amorphous nature. Figure 2(d) depicts the critical fluctuations in B-doped Q-carbon thin films.

The figure indicates the presence of mean-field region (n=-1 and -0.5), and critical region (n=-0.2). The critical fluctuations explicitly explain the curvature of the resistivity plot near T_c.[33] In the mean-field region the reduced conductivity ($\sigma'=\Delta\sigma/\sigma_0$) is expressed by using the Aslamazov-Larkin equation: $\frac{\Delta\sigma}{\sigma_0} = (AT')^n$,[34] where σ_0 is the conductivity at 300 K, $\Delta\sigma$ is the difference between room temperature conductivity and conductivity at a particular temperature, A is the temperature independent constant, n is the critical exponent (n = -0.5 and -1.0 for 3D and 2D critical fluctuations, respectively), and T' is the reduced temperature calculated using the relation: $T' = (T/T_c - 1)$. The critical fluctuations occur extremely close to T_c and the dimensionality of the fluctuations (2D or 3D) are important superconducting parameters. A close observation also indicates that the mean field region starts from 59.9 K which is also the $T_{c\ on}$ state for the B-doped Q-carbon thin films. There is a transition from 2D to 3D nature of critical fluctuation near T_c in the superconducting thin films. The 2D to 3D crossover is observed at T/T_c = 1.02 as compared to T/T_c = 1.11 in other high-temperature superconductors.[33] With decresing temperatures, the 3D fluctuations are therefore predominant in B-doped Q-carbon. Similar nature of 3D fluctuations are also seen in other high-temperature superconductors: YBCO, LSCO.[33] The critical fluctuations measurements also indicate that the $T_{c\ off}$ condition occurs at 55.6 K which is extremely close to the previously calculated value of $T_{c\ off}$. Below the mean field region, the ctitical region starts, indicating the onset of zero-resistivity condition. The presence of these critical fluctuations show moderate to strong electron-phonon coupling in the superconducting state.

C. Magnetic flux creep: Figure 3 depicts the isomagnetic time-dependent magnetic moment measurements in B-doped Q-carbon thin films at different temperatures (5, 20, 30, 40, and 45 K). The flux creep measurements are performed at a high magnetic field (1 T, field below upper

critical field) which facilitates a strong interaction between the dense magnetic vortices. These measurements are also known as magnetic flux creep where the propagation of flux field lines (magnetic vortices) with increasing time at isothermal and isomagnetic conditions are observed. The flux creep phenomenon in the superconducting thin films follows the Anderson-Kim logarithmic time dependence.[35] The reduced magnetic moment (*M(t)/M(t=0)*) *vs* time (in log scale) plots are shown in figure 3(a). The decrease in the value of reduced magnetic moment with time indicates that the motion of the pinned magnetic fluxes is associated with the flux creep which is activated thermally (k_BT). The plots also indicate that the probability of the thermally activated jumps increases exponentially with an increase in temperature. It is also known that the thermally activated creep mechanism leads to dampening of supercurrents and reduction of magnetization. Therefore, large flux creep thwarts the high-temperature (near T_c) use of superconductors. As it is evident from the time-dependent reduced magnetic moment plot that there is only ~4% decrease in the magnetic moment at 45 K (and 1 T). Therefore, there exists a strong pinning potential (discussed below) in B-doped Q-carbon thin films which restrict the thermally activated creep mechanism. An extremely low decrease of magnetic moment with increasing time, indicates the immense applicability of B-doped Q-carbon thin films in MRI and NMR inserts. A much higher change in magnetic moment (~20%) is observed in other high-temperature superconductors due to the formation of a frustrated glassy state.[36] The time-dependent magnetic moment data in the superconducting thin films are fitted using the Anderson-Kim logarithmic equation: $\frac{M(t)}{M(t=0)} = 1 - S \times \ln\left(1 + \frac{t}{\tau_0}\right)$, where τ_0 denotes the time constant and S denotes the isothermal magnetization relaxation. The values of pinning potential (at different temperatures) can be calculated by using the equation: $U_p = {k_BT}/{S}$. The Anderson-Kim fitted plots are shown in the figure 3(a) for various values of T/T_c. The critical parameters

which govern the flux creep phenomenon are the pinning potential, isothermal magnetization relaxation, and time constant. Figure 3(b) indicates an exponential dependence of the isothermal magnetization relaxation with reduced temperature (T/T_c). The exponenential relation between S and T_c is calculated as: $S \approx (e^{T/0.07T_c})$. The plot indicates that after a T/T_c value of 0.7, there occurs a massive thermally activated flux creep in the B-doped Q-carbon thin films. The thermally activated creep is associated with the average velocity of the thermally activated jumps (of magnetic flux lines) which are exponentially related to temperature. The temperature-dependent isothermal magnetization studies indicate a strong flux creep near T_c. The strong thermal fluctuations near T_c also create a vortex liquid state thereby reducing the effective pinning potential (shown in inset of figure 3(b)). At 5 K, the pinning potential is calculated as 0.14 eV which is comparable to various non-BCS high-temperature oxide superconductors.[37] It is also observed that there is a minimal change of pinning potential with temperature (up to T/T_c = 0.6). In most of the superconductors the thermally activated creep starts at low temperatures unlike in B-doped Q-carbon (due to the presence of homogeneosly dispersed pinning centers). In high-temperature oxide (BCS as well as non-BCS) superconductors, the pinning centers are formed due to the presence of strain or non-superconducting phases, which require addition of external non-magnetic impurities.[37] In B-doped Q-carbon, the B-doped sp^2 hybridized carbon entities form the effective pinning centers. The B-doped sp^2 entities are situated at the interface of B-doped sp^3 structures. The details of the geometrical modeling of these superconducting phases can be found elsewhere.[38] These electronic states are formed as a result of the ultrafast melting and quenching process of molten B and C. Therefore, these pinning centers are uniformly distributed throughout the B-doped Q-carbon structure. This increases the potential applications of B-doped Q-carbon thin films in superconducting pumps, transmission lines, and

MAGLEV tracks. The inset in figure 3(b) also indicates the temperature-dependent time constant measurements in the novel superconducting thin films. The time constant determines a transient state before the onset of the logarithmic magnetic relaxation. A transient time of ~400 sec is registered at temperatures close to T_c which indicates a superior superconducting behavior of B-doped Q-carbon thin films. Below the superconducting transition temperature, the magnetic flux lines extend over a distance approximately equal to the London penetration depth which is 59.4 Å in B-doped Q-carbon thin films. The free energy barrier (ΔF near 0 K) of the flux bundle can be calculated as 793.14 T^2 nm^3 using the equation:$\Delta F = (\frac{H_{c2}(0)^2}{8\pi})\lambda_L{}^3$.[39] The large value of free energy barrier of the flux bundle and pinning potential in B-doped Q-carbon thin films cause high values of critical current density. In B-doped Q-carbon thin films, the 3D nature of critical fluctuations (near T_c) and a high pinning potential also result in the butterfly-like hysteresis (in the M-H plots), indicating superior superconducting characteristics of B-doped Q-carbon. Figure 3(c) depicts the superconducting region in B-doped Q-carbon, which is enclosed by T_c, H_{c2}, and J_c. The three vertices of figure 3(c) illustrate T_c (55.0 K), J_c (7.10×10^8 A/cm^2), and H_{c2} (9.75 T), which are the three important parameters of a superconducting material. Outside the superconducting region, the material is in the normal (conducting) state.

D. Structure-property correlations: Figure 4(a) indicates high-resolution SEM image of superconducting B-doped Q-carbon thin films. The B-doped Q-carbon is formed near the sapphire interface, above which quenched carbon layer forms after quenching. This layer shows nanoscale cracks exposing the B-doped Q-carbon film underneath. These cracks are formed because of an order of magnitude higher coefficient of thermal expansion of amorphous carbon overlayer than that of the B-doped Q-carbon. The tensile strain ($\Delta\alpha \times \Delta T$) is estimated to be $\sim 5 \times 10^{-6} \times 4000 = 0.02$ or 2%. The cross-sectional HAADF image indicates the formation of the

thin layer of B-doped Q-carbon close to the sapphire substrate where maximum value of undercooling occurs. The B-doped Q-carbon has negative electron affinity and therefore it glows under the application of a stage (voltage) bias. The inset of figure 4(a) shows the formation of diamond at the triple points of the B-doped Q-carbon filamentary structure. The formation of diamond from the highly undercooled B-doped Q-carbon structure occurs by homogeneous nucleation and has <110> out-of-plane orientation. A heterogeneous nucleation of diamond is favored on *c*-sapphire substrate, which has <111> out-of-plane orientation. The cross-sectional HAADF image along with SAED pattern are shown in figure 4(b). The HAADF image shows the formation of ~90 nm thick superconducting B-doped Q-carbon thin film on *c*-sapphire substrate. A layer of Pt is deposited on the top of B-doped Q-carbon to minimize Ga^{3+} damage during focused ion beam operations. The SAED ring pattern conclusively proves that B-doped Q-carbon is amorphous in nature. The intensity profile plot is superimposed on the electron diffraction pattern, which shows the presence of first and second nearest neighbors, corresponding to 111 (center) and 220 (edge) of diamond tetrahedra. This is consistent with our geometrical modeling of these phases.[38] The room-temperature EEL spectroscopy (figure 4(c)) helps us to calculate the B-at% present in the B-doped Q-carbon structure. The EEL spectrum obtained from different points from the B-doped Q-carbon thin film shows the K edges of B and C. The core-loss EEL spectrum from points 1 and 2 depict the characteristic π^* and σ^* peaks of B and C. The π^* and σ^* are the antibonding (high-energy) electronic states of π and σ bondings. The presence of these antibonding electronic states indicates that B and C atoms are present in both sp^3 and sp^2 hybridized states. The similar nature of EEL spectrum from point 1 and point 2 indicates a homogeneous nature of bonding states in the B-doped Q-carbon structure. This is a characteristic of bulk superconductivity needed for practical applications in transmission lines,

MAGLEV tracks, superconducting pumps, *etc.* The EEL spectrum from point 3 (substrate) shows a complete absence of B and C K edges. By using the EELS quantification routine, the B concentration is calculated as 27.0 at% and rest is C (73.0 at%).

Figure 4(d) depicts the unpolarized Raman spectroscopy of as-deposited (before PLA) and B-doped Q-carbon (after PLA) thin films. The Raman spectroscopy is performed at 300 K using 532 nm excitation wavelength. It is clearly evident from the spectrum that there is a significant increase in the sp^3-bonded C fraction (from 0.65 to 0.76) after the nanosecond laser melting and subsequent quenching process. In the range between 1000-1800 cm^{-1} the Raman spectrum can be deconvoluted into three Raman-active vibrational modes. The peaks are centered around 1100, 1300, and 1600 cm^{-1}. The first peak corresponds to sp^2 dangling bonds at the surface of sp^3-bonded entities. The second and third peaks correspond to sp^3 and sp^2 bondings in C, respectively. The undoped phase of ferromagnetic Q-carbon which is formed by nanosecond laser irradiation and subsequent quenching process, contains 75-85% sp^3 bonding and rest sp^2. In the case of B-doped diamond superconducting thin films (T_c = 4 K) a sharp peak centered at 1332 cm^{-1} and a broad graphitic peak at 1560 cm^{-1} are predominantly observed in Raman spectroscopy. Therefore, the Raman spectra for B-doped Q-carbon thin films (T_c = 55 K) are different from that observed in B-doped diamond. This indicates that the sp^3 and sp^2 bonding states play an important role in high-temperature superconductivity. There occurs a quantum mechanical interference between the zone-center Raman active optical phonon and the continuum of electronic states created by B atoms in B-doped Q-carbon. This phenomenon gives rise to asymmetry and red-shift of the Raman-active vibrational modes in the B-doped Q-carbon thin films. The red-shifts (*w.r.t* the as-deposited thin film) in the sp^3 and sp^2 bonded C (in B-doped Q-carbon thin films) are 15.75 and 29.02 cm^{-1}, respectively. The red-shifts also indicate

that B is doped in substitutional sites of sp^3 and sp^2 bonded C. The Raman red-shifts also indicate a large value of electron-phonon coupling which is also calculated using McMillan formula. The B-doping in sp^3 C leads to high-temperature superconductivity *via* the formation of Cooper pairs whereas the B-doping in sp^2 C introduces pinning centers which increase critical current density and decrease the flux creep near T_c. In the case of B-doped diamond superconducting thin films, extra peaks are observed between 400-1200 cm^{-1}.[40] These peaks occur due to maximas in the phonon density of states, which suggest strain-induced distortion in the diamond lattice upon B-doping. The presence of these extra peaks also indicates the presence of B pairs in interstitial sites of diamond which drastically reduce the superconducting transition temperature. The absence of these extra peaks in B-doped Q-carbon suggests that the B atoms are present in the electrically active sites thereby rendering improved superconducting properties (high T_c, J_c, and H_{c2}, and low flux creep). The formation of B-doped Q-carbon thin films occurs *via* liquid phase which explains the presence of B in the electrically active sites of C. The Raman spectroscopy also shows that the deformation potential of the hole states (after B-doping) is caused by the C-C bond stretching (red-shift of Raman peaks).[41] Therefore, phonon coupling is the main cause of high T_c in B-doped Q-carbon thin films.

The electronic Raman spectra of superconducting B-doped Q-carbon and as-deposited B-C thin films are shown in figure 4(e). The results show distinct shallow acceptor energy levels centered at 14.7, 25.0, 36.7, and 46.6 meV in B-doped amorphous Q-carbon, which are not present in the as-deposited thin films. The peak near 420 cm^{-1} corresponds to *c*-sapphire (substrate), which is present in the as-deposited and B-doped Q-carbon thin films. The first electronic Raman peak at 14.7 meV corresponds to 1*s* to 2*s* electronic transition, whereas the other two correspond to 1*s* to 3*s* and 1*s* to 4*s* transitions. The electronic transitions pertaining to

1*s* to 4*s* orbitals are interesting as they are situated extremely close to the valence band maximum (VBM). Previous reports have confirmed that at low B concentrations ($<1\times10^{18}$ cm^{-3}) the electronic transitions pertaining to only $1s(p_{3/2}) \rightarrow 1s(p_{1/2})$ at 16 cm^{-1} occur.[42] The Lyman series electronic transitions corresponding to 1*s* to n*s* transitions (*n* = 2,3, and 4) are observed at higher B concentrations in the substitutional sites of sp^3 bonded C.[42] It has been also observed that at higher B concentrations there occur spin-orbit splitting and therefore two peaks show up which correspond to $p_{3/2}$ and $p_{1/2}$ electronic states. The spin-orbit splitting is found to be 10 meV in the case of B-doped Q-carbon as compared to 6 meV in B-doped diamond. This indicates a significant overlap of the electronic acceptor states in B-doped Q-carbon thereby increasing the density of the electronic states near the Fermi level. Therefore, Raman studies conclusively show that formation of new acceptor states, increase in electronic density of states near E_F, and large electron-phonon coupling cause superior superconducting properties in B-doped Q-carbon thin films.

Figure 4(f) illustrates the peak-fitted π^* and σ^* antibonding electronic states present in the C K edge in B-doped Q-carbon thin films. The sp^3 bonded C is calculated to be 78% (and rest sp^2) which is similar to that calculated from Raman spectroscopy (figure 4(d)). The π^* and σ^* peaks are seen at 283 and 289 eV, respectively. Figure 4(g) depicts the π^* and σ^* antibonding electronic states present in the B K edge in the novel superconducting thin films at 191 and 198 eV, respectively. The K edges of B and C in B-doped Q-carbon thin films are centered at different energy levels and the peak shapes are different as compared to pristine B and C atoms. These indicate a cumulative change in the local (electronic) environment of B atoms caused due to doping in the B-doped Q-carbon structure. The sp^3 bonded B is calculated to be 70% (and the rest is sp^2). Therefore, 19 at% B is present in the sp^3 sites which leads to the formation of

positively charged holes. These holes pair up below the superconducting transition temperature to give rise to high-temperature superconductivity in B-doped Q-carbon thin films. On the other hand, 8 at% B is present in the sp^2 sites which act as pinning centers thereby increasing the values of J_c and H_{c2}. The sp^2 bonded B is also responsible for low flux creep near T_c, thereby facilitating the use of this novel superconducting material in MRI and NMR inserts.

E. Discussion: Previous reports have indicated that T_c rises monotonically with increasing B concentration (in the substitutional sites) in B-doped diamond. The highest value of T_c (11 K) was achieved in diamond-5%B thin films synthesized using PECVD (plasma enhanced CVD) technique.[8] It has also been observed experimentally that the presence of substitutional disorder (with increasing B concentration) can quench T_c in B-doped diamond by opening an energy gap in the valence states. At higher B concentrations, B-doped diamond enters into the dirty type-II BCS superconductor regime where scattering of Bloch states by impurities does not play an important role. Therefore, increasing the T_c by increasing B concentration in the diamond structure beyond the thermodynamic solubility limit is not an optimal solution to attain high-temperature superconductivity. In the case of B-doped Q-carbon, the substitutional B in the diamond tetrahedra, which are randomly packed, does not cause lattice distortion even at concentrations exceeding thermodynamic solubility limits. This ultimately causes high T_c and improved superconducting properties in the B-doped Q-carbon structure. The substitutional B in B-doped Q-carbon acts as shallow acceptor states lying extremely close to the valence band maximum. This gives rise to the formation of holes (Cooper pairs) which strongly couple with the phonons thereby giving rise to high T_c. Increased B concentration from 5 to 27 at% (in the substitutional sites) causes an increase in the electron-phonon coupling strength leading to an increase in the T_c. The density of electronic states near the Fermi energy level is predominantly

characterized by the electronic states in substitutional B atom. Therefore, an increase in the electronic density of states near the Fermi level is directly related to the rise in T_c in heavily doped materials. Theoretical studies have also predicted that in the superhard material, BC_5 with 16.7 at % of B (T_c=38 K), the electronic density of states near the Fermi energy level is 2.1 times higher than that in 2% B-doped diamond (T_c=4 K).[43] The phonon density of states and energy calculations in BC_5 reveal that the higher energy (115-160 meV) and lower energy modes (<100 meV) correspond to C-C and B vibrations, respectively. There is also an increase in the intensity of phonon density of states at low energy level with increasing dopant concentration.[44] Similar nature of the increase in the phonon density of states (at low energy) are also observed in highly B-doped Q-carbon structure from the electronic Raman spectroscopy. The large values of elastic constant and strong chemical bonds in super hard materials leads to the formation of high-energy phonons and increased electronic charge densities which can lead to high T_c.[45] The σ and π band contributions in B-doped Q-carbon give rise to high J_c, H_{c2}, and pinning potential. The upward curvature of the temperature-dependent H_{c1} plot is indicative of π band scattering that leads to low flux creep near T_c in B-doped Q-carbon. The $H_{c1}^{(\sigma)}$ fraction is calculated to be 0.61 from the temperature-dependent H_{c1} plot. This is in excellent agreement with the B σ electronic state fraction (0.70) calculated from the B K edge in EELS. Therefore, the sp^2/sp^3 ratio plays an important role in the superconducting properties of B-doped Q-carbon.

The SLIM (simulation of laser interaction with materials) programming[46] is used to simulate the laser-solid interactions which determine the formation of the novel high-temperature superconducting phase. The SLIM calculations involve an accurate finite difference method to calculate the threshold energy density, melt depth, and solidification velocity of the pulsed laser annealed samples. The threshold energy (E_{th}) required for melting the layers of amorphous C

and B thin film is calculated to be ~0.4 J/cm^2 by using the equation $E_{th} = \frac{K_s T_m \zeta^{0.5}}{(1-R_l)D^{0.5}}$, where K_s is the thermal conductivity of amorphous carbon (=0.3×T$^{-0.53}$ W cm^{-1}K^{-1}), T_m denotes the difference between the substrate temperature of *c*-sapphire and melting temperature of amorphous carbon (=3523 K), $\zeta$is the pulsed laser width (=20ns), R_l denotes the reflectivity of the amorphous carbon at 193 nm (=0.1), and D is diffusivity of amorphous carbon at room temperature (=2 cm^2 sec^{-1}). With the increase in the pulse energy density, there occurs an increase in the thickness of the melted region. Therefore, 0.6 J/cm^2 pulse energy is used to melt the 500 nm composite layer of B and C. As the laser pulse terminates, the melt front recedes back to the surface. The initial stages of solidification see a low velocity but quickly reach the maximum when the steady state condition is achieved. The maximum melt depth (Δx) is calculated by using the equation: $\Delta x = (1-R_l)(E-E_{th})/(C_v T_m + L)$, where, C_v denotes the volume heat capacity of amorphous carbon at its melting point (=2.1 J cm^{-3} K^{-1}), and L is the latent heat of fusion of amorphous carbon (= 19775 J cm^{-3}). The melt in velocity (v_{in}) is calculated using equation: $v_{in} = \frac{LC_1^2}{K_l \zeta}(E-E_{th})^2 K_1 / L\Delta x$, where ΔT denotes the temperature difference between maximum temperature and melting point of amorphous carbon. The homogeneous melt cools down with high solidification velocities (10-20 m/sec). This causes sufficient undercooling (pressure) to form highly dense and B-doped amorphous Q-carbon. The formation of a homogeneous melt (after the super undercooling process) triggers the liquid phase diffusion (diffusivity ~10^{-4} cm^2/sec), where the dopant concentrations can exceed the retrograde thermodynamic solubility limits. Again the growth velocity (v) is directly related to the undercooling by the following equation: $v = \frac{D_\propto f}{\lambda f_D}\left(1 - e^{\frac{(T_m - T_u)\Delta S}{kT}}\right)$, where, $D_\propto, f, \lambda, f_D, k, T,$ T_m, T_u and ΔS denote the liquid diffusivity, fraction of the available sites, atomic jump distance,

geometrical factor associated with diffusion, Boltzmann constant, temperature, melting temperature, undercooling temperature, and the change in entropy, respectively. Therefore, an increase in the value of undercooling favors the formation of the amorphous and highly doped superconducting phase. The increase in B concentration favors the formation of shallow acceptor states near the Fermi level, which cause high temperature superconductivity in amorphous B-doped Q-carbon thin films.

Conclusions:

A type-II BCS superconductivity is experimentally observed in phase-pure B-doped Q-carbon thin films. This novel phase is formed as a result of nanosecond laser melting and subsequent quenching of highly undercooled state of molten B and C. This synthesis process can enhance the dopant concentrations beyond the thermodynamic solubility limits *via* solute trapping. Therefore, the dopants (B) can be incorporated into substitutional (electrically active) sites (of sp^3 bonded C) without affecting their energy levels and ionization efficiencies. The liquid phase diffusivity (~10^{-4} cm^2/sec) of B in C leads to an increase in the atomic concentration of B in C beyond the retrograde thermodynamic solubility limits. The atomic% of B in B-doped Q-carbon thin films is found to be 27.0 as compared to 2.0 in B-doped diamond (T_c = 4 K). Therefore, the increase in B at% plays an important role in increasing the electronic density of states near the Fermi energy level which increases the T_c in B-doped Q-carbon. The superconducting transition temperature and upper critical field (at 0 K) are calculated to be 55.0 K and 9.75 T, respectively. The magnetic moment measurements indicate that the upper and lower critical fields follow $H_{c2}(0)$ $[1-(T/T_c)^{1.77}]$ and $H_{c1}(0)$ $[1-(T/T_c)^{1.19}]$ temperature dependence, respectively. The magnetic moment *vs* temperature plots indicate that a complete shielding occurs when the samples are mounted perpendicular to the field which is also the reason for the 94.5% increase in

the negative magnetic moment at the perpendicular position (as compared to the parallel position). The temperature-dependent lower critical field plot indicates an upward curvature ~0 K which can be explained by the increased sp^2 contribution in the structure of B-doped Q-carbon. The B in sp^2 electronic sites increases the value of pinning potential which reduces the magnetic flux creep near T_c. The value of the electron-phonon coupling in B-doped amorphous Q-carbon is ~ 5 times than that in 2 at% B-doped diamond (T_c=4 K). In B-doped Q-carbon thin films we have observed the onset of superconductivity ($T_{c\ on}$) and zero-resistivity ($T_{c\ off}$) conditions at 59.8 and 55.4 K, respectively. The upper critical field calculated from the electrical measurements is ~10 T. The critical fluctuation measurements indicate that the 2D to 3D crossover occurs at T/T_c = 1.02 (by using the Aslamazov-Larkin equation) which is comparable to other high-temperature superconductors. The magnetic flux creep measurements in B-doped Q-carbon thin films follow the Anderson-Kim logarithmic time dependence. After a T/T_c value of 0.7, there occurs a massive thermally activated flux creep in the superconducting thin films. At low temperatures, the pinning potential is calculated as 0.14 eV which is comparable to various high-temperature oxide superconductors. The B-doped sp^2 hybridized carbon entities form the effective pinning centers which increase the potential applications of B-doped Q-carbon thin films in superconducting pumps, transmission lines, and MAGLEV tracks. The FESEM, HAADF, and SAED pattern indicate the formation of large-area amorphous superconducting thin films. The EELS and Raman spectroscopy of B-doped Q-carbon thin films illustrate that ~75% of C exists in the sp^3 bonded state (and rest is sp^2). The presence of the antibonding electronic states in EELS indicate that B and C atoms are present in both sp^3 and sp^2 hybridized states. The detailed EELS quantification reveals that 70% of B exists as sp^3 and therefore 20 at % of B is doped in the sp^3 electronic states of Q-carbon. This causes the formation of positive

holes, resulting in superconductivity below 55 K. The Raman spectroscopy indicates a red-shift of Raman active modes in B-doped Q-carbon thin films. This indicates a large value of electron-phonon coupling which is also calculated using the McMillan formula. The electronic Raman spectra of B-doped Q-carbon thin films reveal an acceptor energy level at ~46 meV with the spin-orbit splitting energy value of ~10 meV. The presence of this electronic state near the valence band maximum indicates an increase in the density of shallow acceptor electronic states near the Fermi energy level. Therefore, the strong electron-phonon coupling and increase in the density of states attribute to the high T_c in the novel material. The large values critical current density (~10^8 A/cm^2) in B-doped Q-carbon and their dependence with temperature and magnetic field indicate potential applications. The values of critical current densities are significantly high as compared to typical oxide superconductors (BSCCO ~10^5 Acm^{-2} at 4.2 K), which are important consideration for practical applications. This discovery of high-temperature superconductivity in phase-pure B-doped Q-carbon thin films will stimulate further research in strongly-bonded carbon-based materials in the search for near room temperature superconductivity.

Acknowledgments

We are grateful to Fan Family Foundation Distinguished Chair Endowment for J. Narayan. This work was performed under the National Science Foundation (Award number DMR-1560838). We used Analytical Instrumentation Facility (AIF) at North Carolina State University, which is supported by the State of North Carolina. We are very grateful to Prof. Paul Chu and Dr. Liangzi Deng (Texas Center for Superconductivity, Houston, USA) who reproduced the data shown in figure 1(a) (from our sample). We also acknowledge the useful discussions with Prof Marvin Cohen of University of California, Berkeley, USA.

References:

1 J. E. Moussa and M. L. Cohen, *Phys. Rev. B*, 2008, **77**, 064518.

2 Y. Yang, G. Fedorov, J. Zhang, A. Tselev, S. Shafranjuk and P. Barbara, *Supercond. Sci. Technol.*, 2012, **25**, 124005.

3 A. Gauzzi, S. Takashima, N. Takeshita, C. Terakura, H. Takagi, N. Emery, C. Hérold, P. Lagrange and G. Loupias, *Phys. Rev. Lett.*, 2007, **98**, 067002.

4 Z. K. Tang, L. Zhang, N. Wang, X. X. Zhang, G. H. Wen, G. D. Li, J. N. Wang, C. T. Chan and P. Sheng, *Science,* 2001, **292**, 2462.

5 I. Takesue, J. Haruyama, N. Murata, S. Chiashi, S. Maruyama, T. Sugai and H. Shinohara, *Phys. C Supercond. its Appl.*, 2007, **460**, 111–115.

6 K. Tanigaki, T. W. Ebbesen, S. Saito, J. Mizuki, J. S. Tsai, Y. Kubo and S. Kuroshima, *Nature*, 1991, **352**, 222–223.

7 R. Mitsuhashi, Y. Suzuki, Y. Yamanari, H. Mitamura, T. Kambe, N. Ikeda, H. Okamoto, A. Fujiwara, M. Yamaji, N. Kawasaki, Y. Maniwa and Y. Kubozono, *Nature*, 2010, **464**, 76–79.

8 H. Okazaki, T. Wakita, T. Muro, T. Nakamura, Y. Muraoka, T. Yokoya, S. Kurihara, H. Kawarada, T. Oguchi and Y. Takano, *Appl. Phys. Lett.*, 2015, **106**, 052601.

9 Y. Cao, V. Fatemi, S. Fang, K. Watanabe, T. Taniguchi, E. Kaxiras and P. Jarillo-Herrero, *Nature*, 2018, **556**, 43–50.

10 A. P. Drozdov, M. I. Eremets, I. A. Troyan, V. Ksenofontov and S. I. Shylin, *Nature*, 2015, **525**, 73–76.

11 E. A. Ekimov, V. A. Sidorov, E. D. Bauer, N. N. Mel'nik, N. J. Curro, J. D. Thompson and S. M. Stishov, *Nature*, 2004, **428**, 542–545.

12 B. Šopík and P. Lipavský, *Diam. Relat. Mater.*, 2012, **21**, 77–82.

13 J. Narayan and A. Bhaumik, *J. Appl. Phys.*, 2015, **118**, 215303.

14 J. Narayan, A. Bhaumik and W. Xu, *J. Appl. Phys.*, 2016, **119**, 185302.

15 D. H. Lowndes, R. F. Wood and J. Narayan, *Phys. Rev. Lett.*, 1984, **52**, 561–564.

16 A. Bhaumik, S. Nori, R. Sachan, S. Gupta, D. Kumar, A. K. Majumdar and J. Narayan, *ACS Appl. Nano Mater.*, 2018, **1**, 807–819.

17 A. Bhaumik, R. Sachan and J. Narayan, *ACS Nano*, 2017, **11**, 5351.

18 A. Bhaumik, R. Sachan, S. Gupta and J. Narayan, *ACS Nano*, 2017, **11**, 11915–11922.

19 A. P. Drozdov, M. I. Eremets, I. A. Troyan, V. Ksenofontov and S. I. Shylin, , DOI:10.1038/nature14964.

20 A. Bhaumik, R. Sachan and J. Narayan, *ACS Nano*, 2017, **11**, 5351–5357.

21 Y. Zhang, S. Johnson, G. Naderi, M. Chaubal, A. Hunt and J. Schwartz, *Supercond. Sci. Technol.*, 2016, **29**, 095012.

22 D. Dew-Hughes, *Low Temp. Phys.*, 2001, **27**, 713–722.

23 L. Bromberg, M. Tekula, L. . El-Guebaly and R. Miller, *Fusion Eng. Des.*, 2001, **54**, 167–180.

24 X. X. Yang, Z. F. Zhou, Y. Wang, R. Jiang, W. T. Zheng and C. Q. Sun, *J. Appl. Phys.*, 2012, **112**, 083508.

25 A. Gurevich, *Phys. C Supercond.*, 2007, **456**, 160–169.

26 M. L. Cohen, *Rev. Mod. Phys.*, 1964, **36**, 240–243.

27 W. G. Spitzer, F. A. Trumbore and R. A. Logan, *J. Appl. Phys.*, 1961, **32**, 1822–1830.

28 L. E. Howarth and J. F. Gilbert, *J. Appl. Phys.*, 1963, **34**, 236–237.

29 Y. Sakai, J. R. Chelikowsky and M. L. Cohen, *Phys. Rev. Mater.*, 2018, **2**, 074403.

30 Y. Sakai, J. R. Chelikowsky and M. L. Cohen, *Phys. Rev. B*, 2018, **97**, 054501.

31 B. Oktem, A. Bozbey, I. Avci, M. Tepe, D. Abukay and M. Fardmanesh, *Phys. C Supercond.*, 2007, **458**, 6–11.

32 W. D. Gregory, *Phys. Rev.*, 1968, **165**, 556–561.

33 N. Sudhakar, M. K. Pillai, A. Banerjee, D. Bahadur, A. Das, K. P. Gupta, S. V. Sharma and A. K. Majumdar, *Solid State Commun.*, 1991, **77**, 529–533.

34 L. G. Aslamasov and A. I. Larkin, *Phys. Lett. A*, 1968, **26**, 238–239.

35 T. Scheike, W. Böhlmann, P. Esquinazi, J. Barzola-Quiquia, A. Ballestar and A. Setzer, *Adv. Mater.*, 2012, **24**, 5826–5831.

36 Y. Yeshurun, A. P. Malozemoff and A. Shaulov, *Rev. Mod. Phys.*, 1996, **68**, 911–949.

37 V. Y. Monarkha, A. G. Sivakov and V. P. Timofeev, *Low Temp. Phys.*, 2014, **40**, 861–863.

38 J. Narayan, A. Bhaumik and R. Sachan, *J. Appl. Phys.*, 2018, **123**, 135304.

39 P. W. Anderson and Y. Ren, *MRS Proc.*, 1989, **169**, 3.

40 P. W. May, W. J. Ludlow, M. Hannaway, P. J. Heard, J. A. Smith and K. N. Rosser, *Diam. Relat. Mater.*, 2008, **17**, 105–117.

41 K.-W. Lee and W. E. Pickett, *Phys. Rev. Lett.*, 2004, **93**, 237003.

42 S. N. Polyakov, V. N. Denisov, B. N. Mavrin, A. N. Kirichenko, M. S. Kuznetsov, S. Y. Martyushov, S. A. Terentiev and V. D. Blank, *Nanoscale Res. Lett.*, 2016, **11**, 11.

43 M. Calandra and F. Mauri, *Phys. Rev. Lett.*, 2008, **101**, 016401.

44 Z. Yamani, D. H. Ryan, J. M. Cadogan, F. Canepa, A. Palenzona and A. Orecchini, *J. Phys. Conf. Ser.*, 2012, **340**, 012074.

45 P. B. Allen and R. C. Dynes, *Phys. Rev. B*, 1975, **12**, 905–922.

46 R. K. Singh and J. Narayan, *Mater. Sci. Eng. B*, 1989, **3**, 217–230.

Figures:

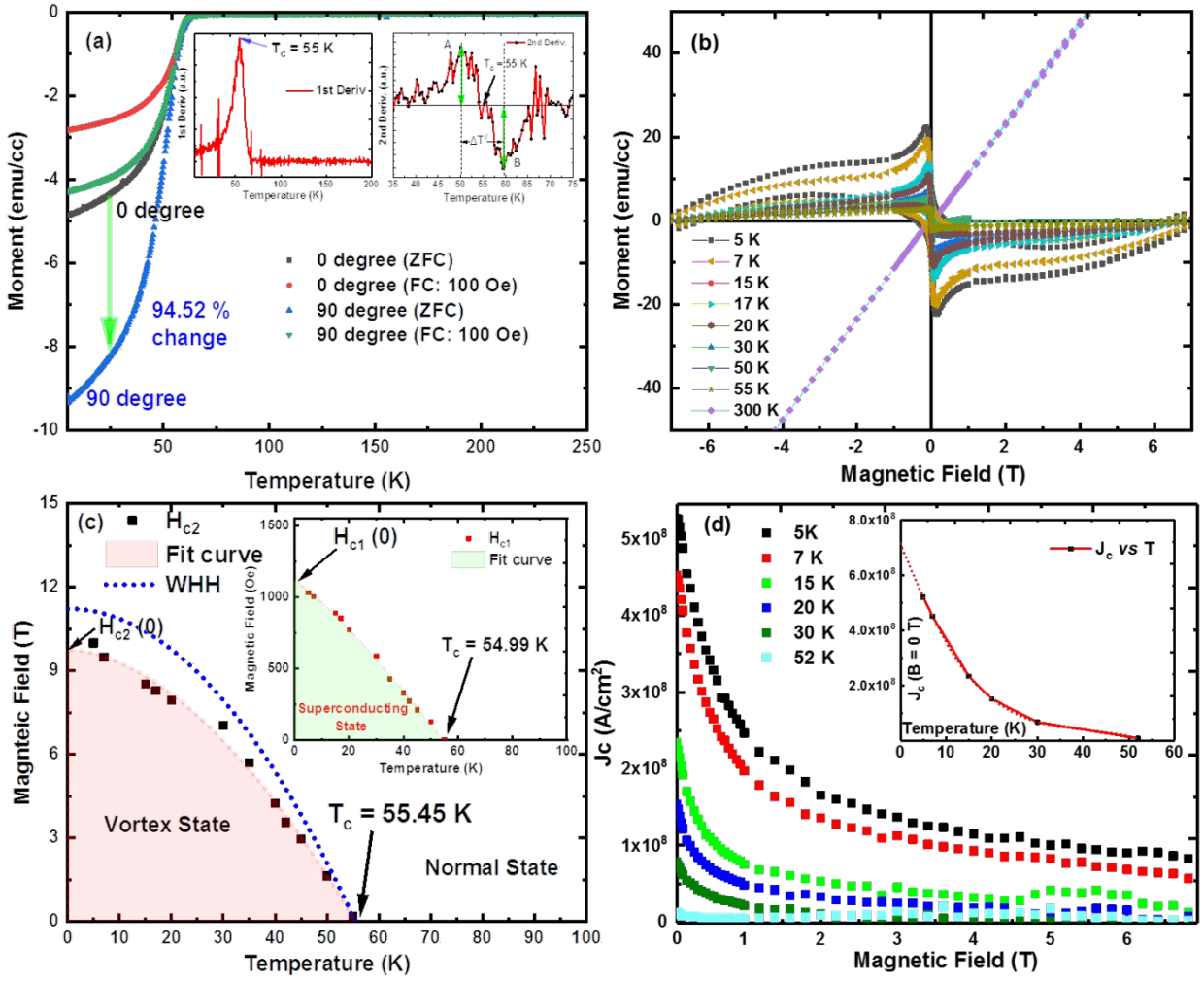

Figure 1: *Magnetic characteristics of B-doped Q-carbon thin films* (a) Magnetic moment *vs* temperature plots for 0 and 90 degree orientations, (b) Magnetic moment *vs* field at various temperatures, (c) Magnetic field *vs* temperature plots showing upper critical field and lower critical field (in the inset), (d) Critical current density *vs* magnetic field plots at various temperatures with the inset showing critical current density *vs* temperature plots at B = 0 T.

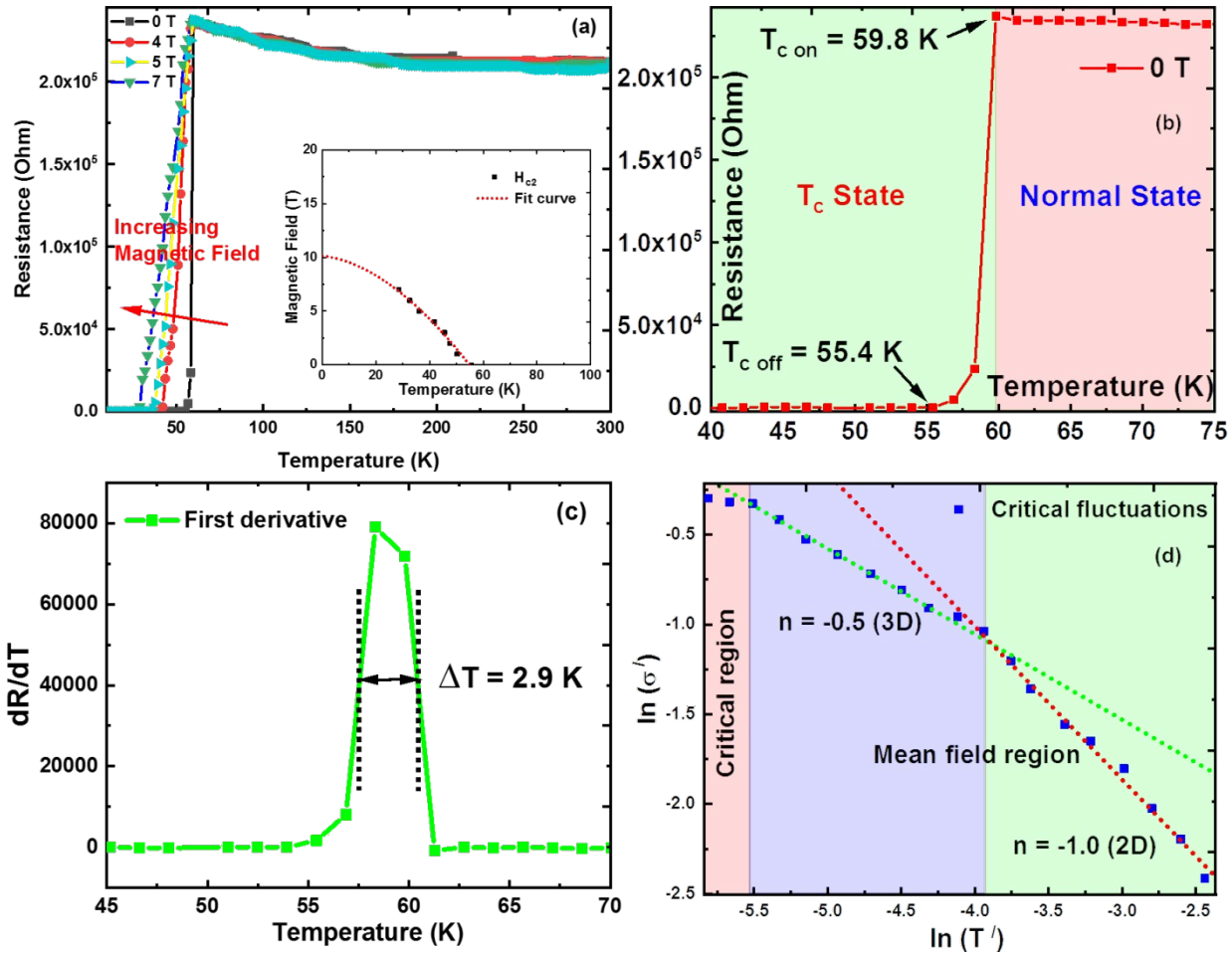

Figure 2: *Electrical characteristics of B-doped Q-carbon thin films* (a) Resistance *vs* temperature plots at different magnetic fields with the inset showing the upper critical field *vs* temperature plot, (b) Resistance vs temperature plot at B = 0 T showing the $T_{c\,on}$ and $T_{c\,off}$ states, (c) First derivative plot showing the transition width as 2.9 K, and (d) Critical fluctuation measurements showing 2D to 3D crossover at $T/T_c = 1.02$.

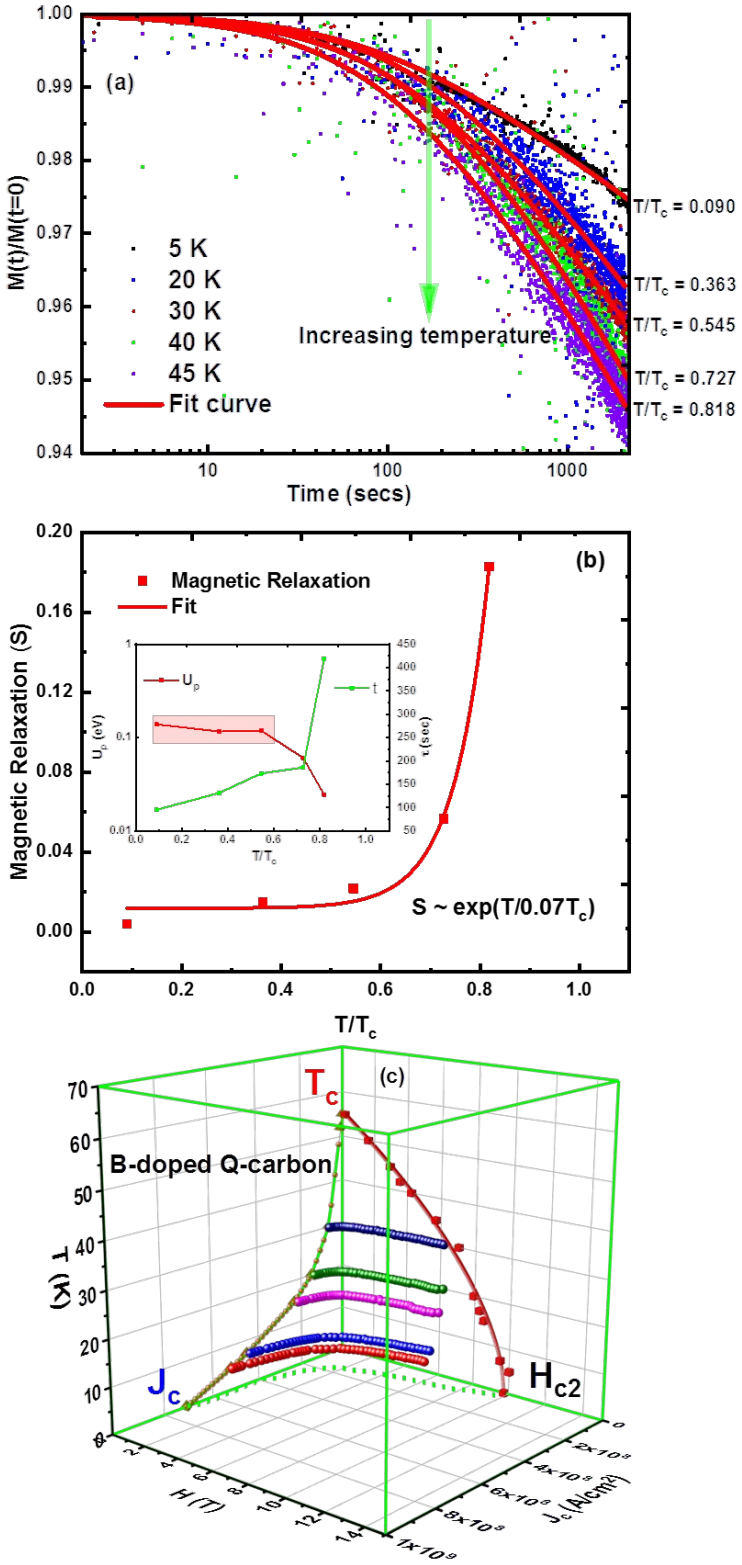

Figure 3: *Magnetic flux creep of B-doped Q-carbon thin films* (a) Time-dependent reduced magnetic moment at various temperatures, (b) Isothermal magnetization relaxation *vs* reduced temperature plots with the inset showing pinning potential and time constant *vs* reduced temperature, and (c) 3D plot of the superconducting region.

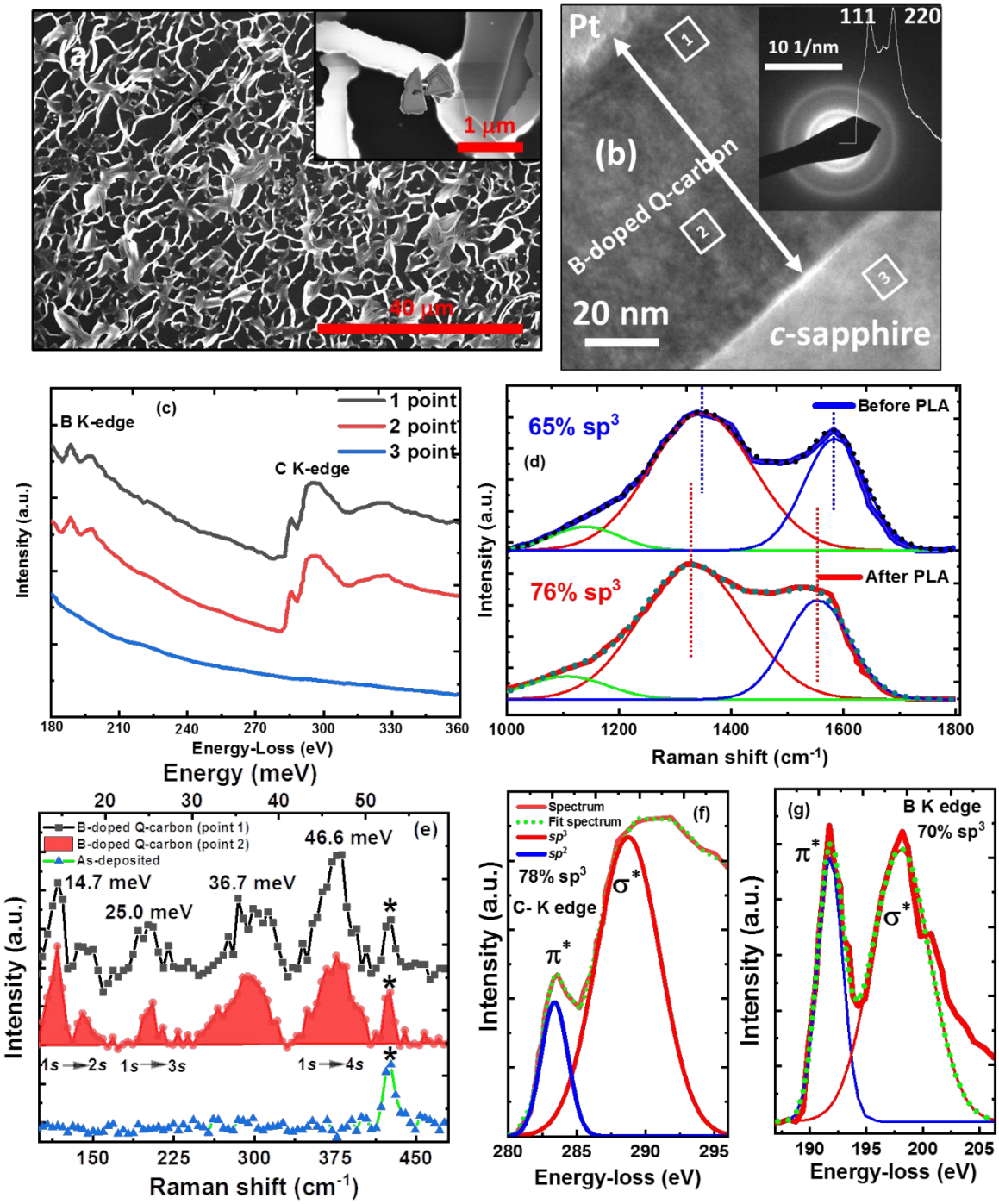

Figure 4: Structural characterizations of B-doped Q-carbon thin films (a) FESEM of B-doped Q-carbon with the inset showing nucleation of diamond at the triple points, (b) HAADF image of B-doped Q-carbon formed on *c*-sapphire substrate with the inset showing SAED pattern of amorphous B-doped Q-carbon, (c) Room-temperature EEL spectra from various points on the HAADF image showing B and C K edges, (d) Raman spectra showing sp^3/sp^2 bonding states in as-deposited and B-doped Q-carbon thin films, (e) Electronic Raman spectra showing the shallow acceptor states near the valence band maximum, (f) and (g) High-resolution EEL spectrum of C and B K edges, respectively.

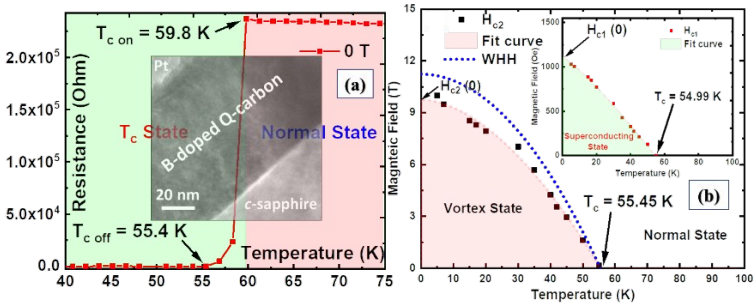

This discovery of record BCS T_c=55 K superconductivity in phase-pure B-doped Q-carbon will provide the pathway to achieve room-temperature superconductivity.